Acta Crystallographica Section D
Biological Crystallography
ISSN 0907-4449

High-resolution powder X-ray data reveal the T_6 hexameric form of bovine insulin

Irene Margiolaki,[a]* Anastasia E. Giannopoulou,[a] Jonathan P. Wright,[b]* Lisa Knight,[b] Mathias Norrman,[c] Gerd Schluckebier,[c] Andrew N. Fitch[b] and Robert B. Von Dreele[d]

[a]Department of Biology, Section of Genetics, Cell Biology and Development, University of Patras, GR-26500 Patras, Greece, [b]European Synchrotron Radiation Facility, BP 220, F-38043 Grenoble CEDEX 9, France, [c]Diabetes Protein Engineering, Novo Nordisk A/S, Novo Nordisk Park, 2760 Maløv, Denmark, and [d]Advanced Photon Source, Argonne, IL 60439, USA

Correspondence e-mail: imargiola@upatras.gr, wright@esrf.fr

Received 19 December 2012
Accepted 8 February 2013

PDB Reference: T_6 hexameric insulin, 4idw

A series of bovine insulin samples were obtained as 14 polycrystalline precipitates at room temperature in the pH range 5.0–7.6. High-resolution powder X-ray diffraction data were collected to reveal the T_6 hexameric insulin form. Sample homogeneity and reproducibility were verified by additional synchrotron measurements using an area detector. Pawley analyses of the powder patterns displayed pH- and radiation-induced anisotropic lattice modifications. The pronounced anisotropic lattice variations observed for T_6 insulin were exploited in a 14-data-set Rietveld refinement to obtain an average crystal structure over the pH range investigated. Only the protein atoms of the known structure with PDB code 2a3g were employed in our starting model. A novel approach for refining protein structures using powder diffraction data is presented. In this approach, each amino acid is represented by a flexible rigid body (FRB). The FRB model requires a significantly smaller number of refinable parameters and restraints than a fully free-atom refinement. A total of 1542 stereochemical restraints were imposed in order to refine the positions of 800 protein atoms, two Zn atoms and 44 water molecules in the asymmetric unit using experimental data in the resolution range 18.2–2.7 Å for all profiles.

1. Introduction

Insulin is a hormone that is highly important in the procedures of fat and glucose metabolism and, consequently, in the treatment of diabetes. Prior to the production of biosynthetic human insulin, therapeutic insulin formulations could be derived from other mammals, as there are only minor differences in the amino-acid sequences. Bovine insulin differs in sequence from porcine insulin at positions A8 (bovine, Ala; porcine, Thr) and A10 (bovine, Val; porcine, Ile) and porcine insulin differs from human insulin at position B30 (human, Thr; porcine, Ala). Although the difference in the bovine sequence from those of human or porcine insulin is minor, it is sufficient to produce an immune response in some individuals. It has been shown that from a therapeutic point of view bovine insulin has a superior pharmacodynamic profile (Seigler *et al.*, 1991). This may arise from a slower dissolution rate of the microcrystals to release insulin hexamers into solution, a slower rate of dissociation of dissolved hexamers to release hormonally active insulin monomers, or both (Smith *et al.*, 2005).

Bovine insulin consists of two chains, A (21 amino acids) and B (30 amino acids), held together by two disulfide bonds, while an extra disulfide bond links CysA6 to CysA11. The A chain consists of two α-helical segments connected by an extended section of polypeptide chain, while the B chain consists of two extended segments connected by a central

α-helical segment. It is known that insulin is characterized by a highly polymorphic nature, which reveals itself under different crystallization conditions such as pH variation (Norrman *et al.*, 2006; Norrman, 2007). Insulin in its hexameric form can adopt three different conformations depending on the presence of phenolic derivatives and the concentration of anions in the crystallization solution. These are denoted as T_6 (Baker *et al.*, 1988; Smith *et al.*, 2003), $T_3R_3^f$ (Ciszak & Smith, 1994; Whittingham *et al.*, 1995) and R_6 (Derewenda *et al.*, 1989; Smith & Dodson, 1992), and each corresponds to a distinct conformation of amino acids B1–B19 in the insulin hexamer (Kaarsholm *et al.*, 1989). Long-lasting therapeutic forms of insulin such as Ultralente are microcrystalline suspensions of hexameric zinc insulin that provide a basal level of insulin for the control of diabetes. Previous powder diffraction results on human Ultralente insulin showed that microcrystals grown in the presence of 1.2 *M* sodium chloride are of the $T_3R_3^f$ conformation, but that the dilution to 0.12 *M* sodium chloride for therapeutic preparations induces the R→T transition, resulting in T_6 hexamers (Richards *et al.*, 1999).

The use of X-ray powder diffraction crystallography, a method which has previously been employed for solving and refining small protein structures from microcrystals and high-resolution synchrotron data, can be beneficial in the identification of distinct insulin polymorphs (Von Dreele, 2003; Margiolaki & Wright, 2008). In recent years, this method has been applied to a considerable range of microcrystalline proteins and is generally considered to be a valuable complementary tool. One of the primary appeals of powder diffraction is that it allows the investigation of protein structure, as well as the screening of different polymorphs, without the requirement for a sizable single crystal, which is usually the limiting step in X-ray crystallography. Instead, powder specimens consist of a large number of randomly oriented diffracting microcrystals, which can be formed easily and, in most cases, in a shorter time period.

High-resolution powder diffraction data are characterized by narrow diffraction peaks, which enable indexing and structure determination (Margiolaki, Wright, Fitch *et al.*, 2007). The first previously unknown protein structure solved and refined from high-resolution X-ray powder diffraction data was that of a variant of T_3R_3 human insulin (Von Dreele *et al.*, 2000). This study was followed by structural determination of the second SH3 domain of ponsin by the molecular-replacement method (Margiolaki, Wright, Wilmanns *et al.*, 2007).

Powder diffraction has already been used for the identification of different crystalline polymorphs of insulin, including T_6, $T_3R_3^f$ and R_6 (Richards *et al.*, 1999). Our previous studies on human insulin cocrystallized with phenol or resorcinol in a wide pH range have revealed several distinct polymorphic forms. In addition, a novel polymorph with monoclinic symmetry ($P2_1$) was identified for both kinds of ligands, displaying similar unit-cell parameters (Karavassili *et al.*, 2012).

In the present study, we use powder diffraction to investigate the anisotropic effects of pH and irradiation time on the lattice parameters of T_6 bovine pancreatic insulin. The anisotropic evolution of the lattice parameters causes a change in the pattern of peak overlaps, allowing the contributing reflections of the overlapped peaks to be partially deconvoluted. The structure is refined using 14 profiles and the flexible rigid-body (FRB) approach. This is the first time that the FRB approach has been applied for the refinement of a protein structure using powder diffraction data.

2. Experimental

2.1. Crystallization

Bovine insulin was purchased from Sigma–Aldrich Chemical Co. (product No. I-6634, Lot 064K10845; CAS No. 11070-73-8). The method of batch crystallization was used to produce polycrystalline samples of T_6 hexameric insulin $\{Zn_2[(AB)_2]_3\}$. During preliminary experiments the salt concentration was varied between 0.2 and 0.35 *M*; buffers were prepared in the pH range 5.9–7.7 by combining pre-prepared 0.5 *M* solutions of sodium monobasic monohydrate phosphate and sodium phosphate dibasic, which were then tested with a pH meter to ensure accurate values. A range of five values were selected and calculated amounts were introduced into the wells of a 24-well crystallization plate containing 10 mg insulin in each well (25 mg ml^{-1}).

During subsequent experiments the salt concentration was kept constant at a molarity that optimized microcrystal

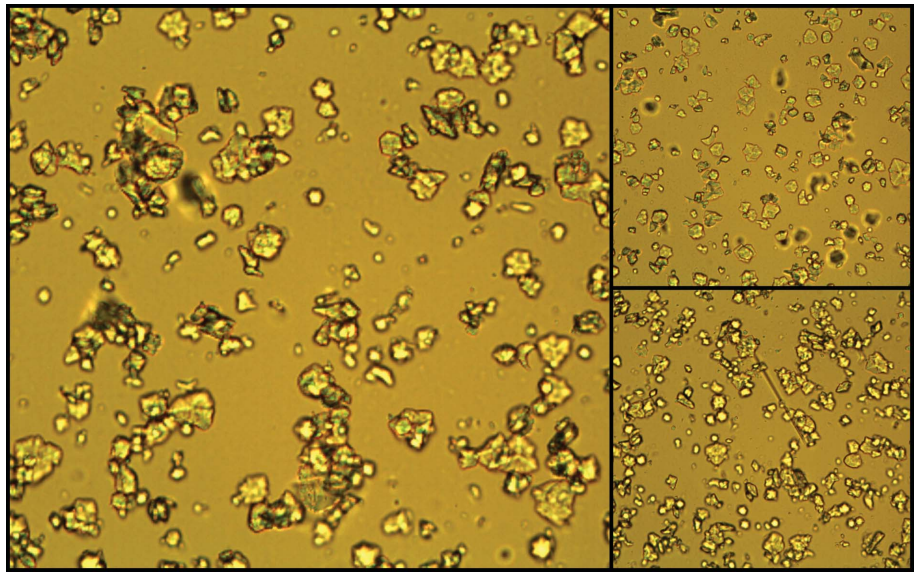

Figure 1
Optical microscopy images of polycrystalline T_6 bovine insulin prepared at RT and the following pH values: 6.8 (left panel), 6.2 (lower right panel) and 5.4 (upper right panel).

formation as observed from the preliminary crystallization screens. Buffers corresponding to the pH range 5.0–7.8 were prepared by mixing different ratios of 0.2 *M* solutions of sodium monobasic monohydrate phosphate (EC No. 2314492) and potassium phosphate (EC No. 2318345) purchased from Hampton Research (Lot 222316). Insulin samples were crystallized at different pH values between 5 and 7.8 in a systematic manner with steps of roughly 0.2 pH units. The protein concentration was kept constant at 25 mg ml^{-1} for all samples. Mixing the buffer solutions with insulin in 24-well crystallization plates resulted in immediate precipitation (Fig. 1).

2.2. X-ray data collection and processing

For the large unit cells typical of proteins, the choice of the instrumental configuration is a key issue (Margiolaki, Wright, Fitch *et al.*, 2007). The best-quality diffraction profiles, in terms of minimum peak widths to reduce peak overlap, data resolution (*d*-spacing) and signal-to-noise ratio, are often obtained at high-resolution synchrotron instruments with parallel beam geometry (equipped with analyzer crystals and point detectors). On the other hand, area detectors allow full powder rings to be recorded and integrated, yielding gains in detection efficiency of more than 10^3 and leading to a drastic reduction in exposure times and radiation damage, thus making measurements on much smaller samples possible. The greatest advantage of using area detectors is that the solid angle for intensity integration increases with scattering angle, resulting in improved intensity statistics in the high-angle region of the powder data. However, they do not provide peak-width resolution that matches the intrinsic peak widths of a protein powder pattern.

In this case, two beamlines at the European Synchrotron Radiation Facility (ESRF; France) were employed in order to maximize the information content of the collected profiles. We selected the high-resolution powder diffraction beamline ID31 (Fitch, 2004), equipped with nine Si(111) analyser crystals, and the materials science beamline ID11, equipped with an area detector. High angular resolution data were obtained on ID31. The samples were loaded in spinning glass capillaries of 1.0 mm in diameter mounted on the axis of the diffractometer and patterns were measured with a period of 1.0 min using a beam size of 1.5 mm^2 (1.5 mm horizontal × 1.0 mm vertical) and a photon flux on the sample of $\sim 3 \times 10^{12}$ photons s^{-1}. The capillaries were centrifuged to achieve better packing of the crystals, which also helped with the removal of excess mother liquor. The capillaries were sealed with wax to prevent subsequent solvent evaporation and the samples were mounted on a translating fast capillary spinner positioned on the axis of the diffractometer. Spinning ensured that even with the rapid data-collection performance of this beamline, good powder averaging was still achieved. Approximately ten scans were collected per sample, translating periodically, at room temperature and a wavelength of 1.29967 (9) Å. Appreciable changes were observed in the data after several patterns had been collected and these are discussed in §3. In order to increase the counting statistics without compromising the data quality, identical scans collected from fresh parts of the samples were summed together. Our previous work has shown that cryocooling of protein powders often leads to microstrains and considerable broadening of the diffraction peaks (Jenner *et al.*, 2007), analogous to the increased mosaicity observed in single-crystal studies (Garman, 1999). Measurements under cryocooled conditions have been performed during recent years and results from selected human insulin

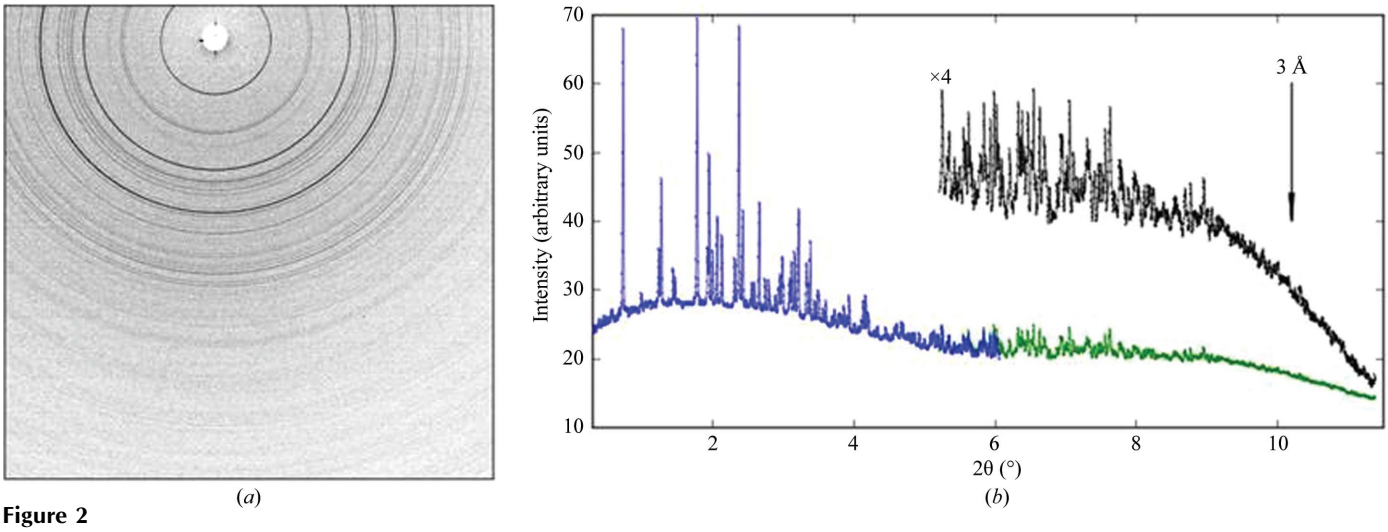

(*a*) (*b*)

Figure 2
(*a*) Low-angle region of the area-detector image of a T_6 bovine insulin polycrystalline sample prepared at pH 5.8. The data were collected with an exposure time of 1 min at RT [ID11, λ = 0.53395 (20) Å]. In the two-dimensional image masked pixels were interpolated from neighbouring values but were excluded from the radial integration. The smooth rings observed in this case show that the sample is close to being an ideal powder, *i.e.* there is no preferred orientation of the microcrystals, which would produce intensity variations around the rings, and no evidence of larger crystallites giving dominant diffraction spots. (*b*) One-dimensional powder diffraction patterns obtained after radial integration of the collected two-dimensional images *via Fit2D* (Hammersley, 1997). The blue and green lines correspond to the low-angle and high-angle data, respectively, collected at two different vertical positions of the area detector (see §2.2). The high-angle data have been expanded by a factor of four at Bragg angles larger than 5° in order to illustrate the presence of diffraction peaks up to ∼3 Å resolution.

polymorphs have been presented elsewhere (Watier, 2011; Watier *et al.*, 2009). In this study, all data presented have been collected at room temperature in order to retain the narrow diffraction lines and to reduce the peak-overlap problem.

Additional measurements were performed on the materials science beamline ID11 at the ESRF using an area detector. The samples were mounted using both borosilicate glass capillaries (as above) and Kapton capillaries as described by Von Dreele (2006). Data were collected from a relatively small sample volume (∼5 µl) at room temperature and a wavelength of 0.53395 (20) Å. The beam was focused using lenses (Vaughan *et al.*, 2011) on the surface of a Frelon4M 2k × 2k CCD camera with a 50 × 50 µm pixel size (Labiche *et al.*, 2007). The sample-to-detector distance was 794.7 mm and was calibrated using silver behenate (Huang *et al.*, 1993). A series of images was collected with 1 min exposures at room temperature (RT) and these were compared in order to monitor any radiation damage. To improve the range of the data while retaining good angular resolution, the detector was also moved vertically to record separate images for the high-angle region. In a powder diffraction measurement, all of the Laue conditions are satisfied simultaneously by different microcrystals which are randomly oriented in the sample. The three-dimensional pattern of Bragg peaks in reciprocal space collapses onto a series of concentric rings (Fig. 2*a*). Each ring represents a set of reflections corresponding to a particular *d*-spacing in the sample. The smooth rings that are observed in this case show that the sample is close to being an ideal powder, *i.e.* there is no preferred orientation of the microcrystals, which would produce intensity variations around the rings, and no evidence of larger crystallites giving dominant diffraction spots. The two-dimensional images were transformed into one-dimensional powder diffraction patterns *via* *Fit2D* (Hammersley, 1997; Fig. 2*b*). The blue trace corresponds to the image as shown and the green trace was produced when the detector was shifted vertically. Similar patterns were then merged to enhance counting statistics. In addition, the area-detector data (ID11) verified the reproducibility of our high-resolution measurements (ID31) and the sample homogeneity.

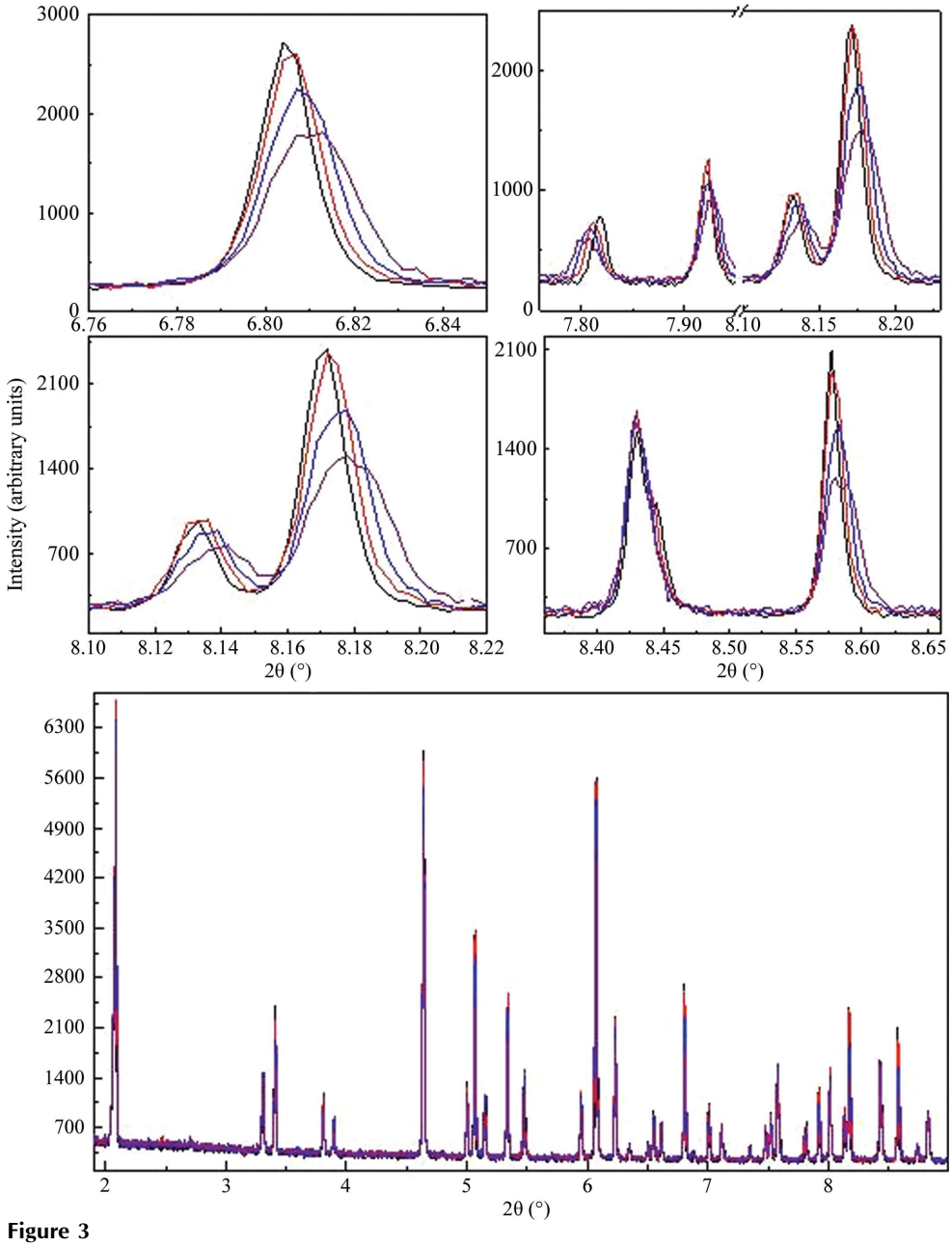

Figure 3
Subsequently collected high-resolution powder diffraction profiles showing gradual sample radiation damage with increasing exposure time to the synchrotron beam. The figure shows magnifications of selected 2θ regimes collected for T_6 bovine insulin (space group *R*3) pH 7.6 at exposure times of 1 min (black line), 2 min (red), 3 min (blue) and 4 min (purple). The unit-cell parameters extracted from the data set collected after 1 min of exposure are a = 82.2823 (4), c = 33.7904 (9) Å. The data were collected at 295 K [ID31, λ = 1.29967 (9) Å].

The patterns were all indexed using *DICVOL* (Boultif & Louër, 1991) incorporated into the *DASH* software package (David *et al.*, 1998) using the fitted positions of the first 20 reflections of the powder diffraction profiles collected for all samples. For instance, a hexagonal unit cell

was found for the sample crystallized at pH 5.0 (space group *R*3; unit-cell parameters $a = 82.59$, $c = 33.60$ Å). This unit cell is in agreement with the expected hexagonal insulin phase crystallized under these conditions corresponding to the T_6 hexameric insulin form (Smith *et al.*, 2005). In order to obtain reliable values of the lattice parameters and to characterize the peak shape and background coefficients without a structural model, Pawley fits (Pawley, 1981) were then performed using the *PRODD* profile-refinement program (Wright & Forsyth, 2000). Finally, stereochemically restrained structure refinement using the Rietveld method (Rietveld, 1969), the FRB approach (as described in §5) and multiple profiles was performed with the *General Structural Analysis Software* (*GSAS*; Larson & Von Dreele, 2001) using the *EXPGUI* graphical user interface (Toby, 2001).

3. Radiation- and pH-induced anisotropic lattice modifications

The various effects caused by exposing samples to an intense X-ray beam are widely discussed topics in single-crystal protein crystallography, since they can seriously hamper structure determination (Garman & Nave, 2002). One common phenomenon is an irreversible radiation-induced lattice expansion, although the mechanism by which this occurs is not fully understood (Ravelli *et al.*, 2002). In many cases, lattice changes are anisotropic and can thus be exploited to improve the resolution of overlapping reflections in a powder pattern (Basso *et al.*, 2005; Von Dreele, 2007; Besnard *et al.*, 2007; Margiolaki, Wright, Wilmanns *et al.*, 2007; Wright *et al.*, 2008; Basso *et al.*, 2010; Helliwell *et al.*, 2010). In the case of powder diffraction data, significant changes in the lattice parameters accompanied by a gradual increase of peak broadening and a significant loss of intensity are common characteristics of radiation-damage effects (Margiolaki, Wright, Wilmanns *et al.*, 2007). For bovine insulin, several powder patterns were collected consecutively from the same sample volume. Each pattern therefore corresponds to a different exposure to X-rays. Fig. 3 shows portions of the low-angle region of the powder data of the bovine insulin sample crystallized at pH 7.6, in which variations in peak position and intensity are apparent. Pawley analysis verified that there is no radiation-induced phase transition after 5 min exposure time and all data sets can be interpreted by the structural characteristics of the T_6 insulin form. Fig. 4(*a*) illustrates an anisotropic variation of the hexagonal lattice dimensions

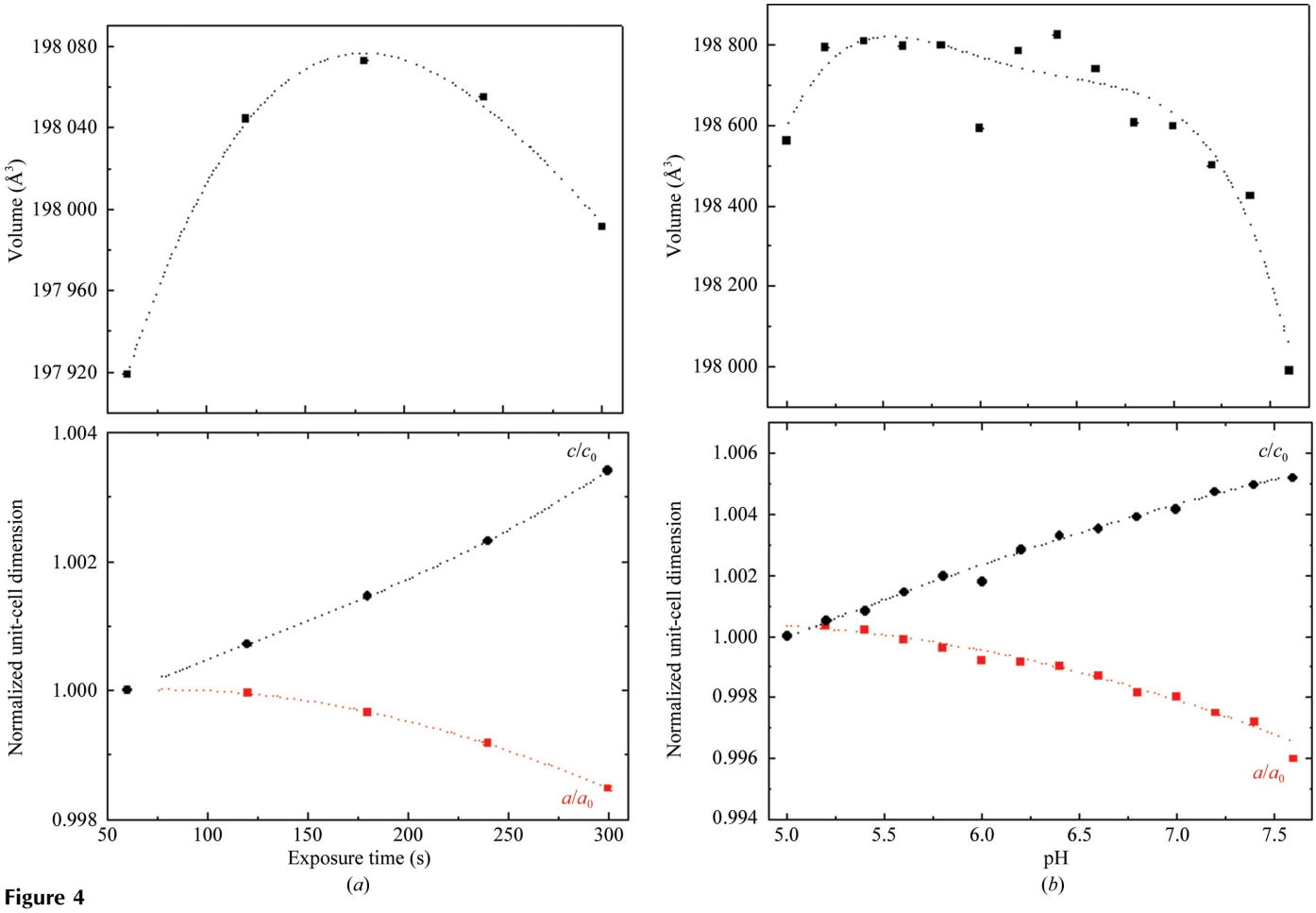

Figure 4
Variation of the unit-cell volume (top) and normalized unit-cell dimensions (bottom) extracted from ID31 data for T_6 bovine insulin (*a*) with increasing exposure time for a sample crystallized at pH 7.6 and (*b*) with the pH of protein crystallization. Note that the error bars are much smaller than the observed variations. The dashed lines are guides to the eye. The refined parameters are listed in Supplementary Tables S1 and S2.

with increasing irradiation time ($\Delta a/a_i = -0.152\%$, $\Delta c/c_i = 0.340\%$, $\Delta V/V_i = 0.0365\%$). The refined unit-cell parameters are listed in Supplementary Table S1[1].

Good-quality polycrystalline samples were obtained in the pH range 5.0–7.6, whereas the sample prepared at pH 7.8 was amorphous. Direct visualization of the 14 collected profiles in a comparative way indicates a clear anisotropic shift of the peak positions with pH (Fig. 5). This observation arises from an anisotropic variation of unit-cell parameters with pH and is quantified *via* Pawley analysis (Supplementary Table S2). Fig. 4(*b*) shows that the crystallographic axis *a* decreases by $\delta a/a_0 = -0.401\%$ and *c* increases by $\delta c/c_0 = 0.518\%$ with increasing pH from 5.0 to 7.6 at RT. Similarly, the decrease in the volume of the hexagonal unit cell is $\delta V/V_0 = -0.286\%$. Fig. 4 indicates a comparable lattice modification with increasing irradiation time and pH. We observe a significant decrease in the *a* axis and increase in the *c* axis in the pH range 5.0–7.6, whereas a less pronounced similar phenomenon is observed with increasing irradiation time from 60 to 300 s. The relatively small changes in the volume of the unit cell in both cases indicate that it is the ratio of the unit-cell parameters in which most of the changes occur (Fig. 4). The observed anisotropic alteration of the unit-cell parameters with pH is analogous to our previous observations on tetragonal HEWL crystallized at 277 K and in the pH range 3.33–6.56 (Basso *et al.*, 2005). In the latter case, the crystallographic axis *a* increases by $\delta a/a_0 = 0.61\%$ and *c* decreases by $\delta c/c_0 = -0.55\%$ with decreasing pH from 6.56 to 3.33 at 277 K. Similarly, the increment in the volume per molecule of the tetragonal unit cell ($Z = 8$) is $\delta V/V_0 = 0.67\%$.

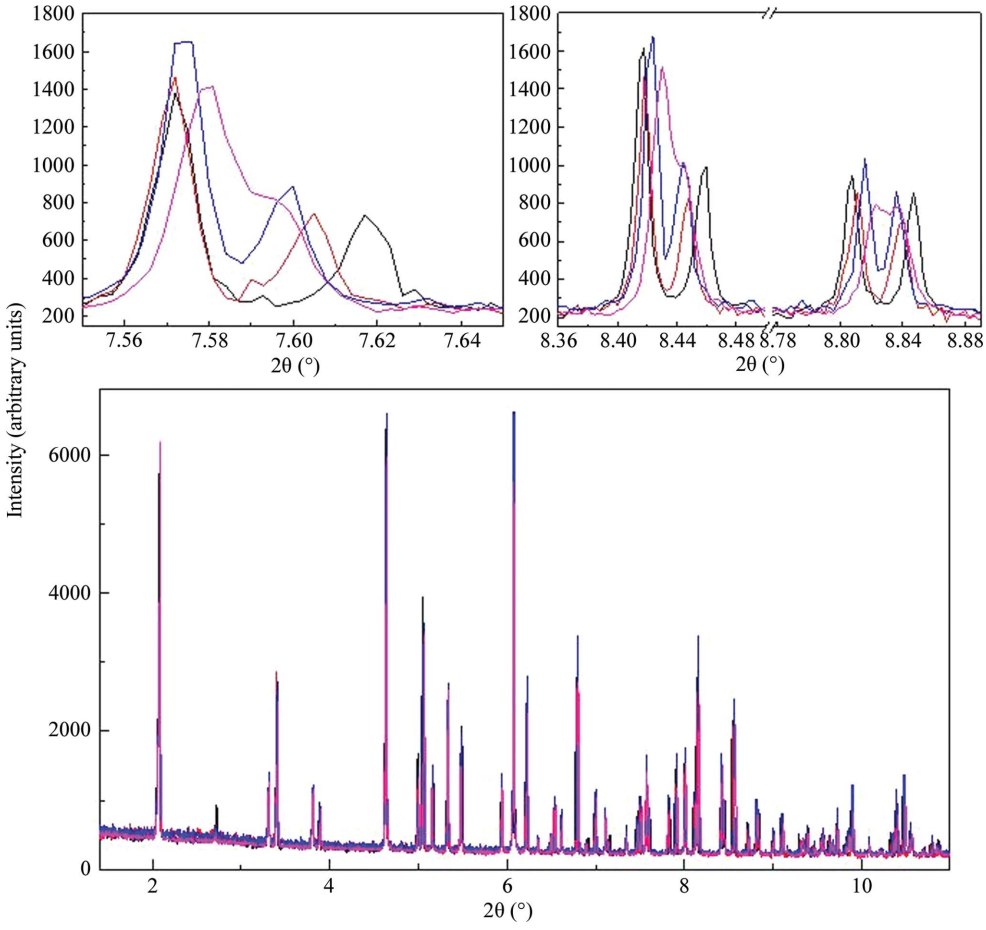

Figure 5
Magnifications of selected 2θ regimes of the high-resolution powder diffraction profiles collected for samples crystallized at pH 5.4 [black line; space group *R*3; $a = 78.8242\ (3)$, $c = 38.15831\ (9)$ Å; $V = 237\ 087\ (2)$ Å^3], pH 6.6 [red line; $a = 79.2996\ (6)$, $c = 37.8911\ (5)$ Å; $V = 238\ 275\ (3)$ Å^3], pH 7.0 (blue line; $a = 79.2996\ (6)$, $c = 37.8911\ (5)$ Å; $V = 238\ 275\ (3)$ Å^3] and pH 7.6 [magenta line; $a = 79.2996\ (6)$, $c = 37.8911\ (5)$ Å; $V = 238\ 275\ (3)$ Å^3]. The data were collected at 295 K [ID31, $\lambda = 1.29967\ (9)$ Å]. This figure illustrates the anisotropic alteration of the lattice dimensions with pH leading to the deconvolution of partially overlapped Bragg reflections.

4. Enhanced intensity extraction from powder diffraction data

Advantage has been taken of the anisotropic peak shifts owing to the pH of crystallization (as described in §3) in order to improve the separation of adjacent peaks and to improve the accuracy of the extracted peak intensities. Therefore, we selected seven profiles with enhanced statistics collected from samples crystallized at pH 5.4, 6.2, 6.6, 6.8, 7.2, 7.4 and 7.6. Intensities were extracted *via* a multi-pattern Pawley refinement, in which each diffraction profile is calculated as a sum of overlapping reflections, the intensities of which are variables in a least-squares procedure. The seven data sets were fitted using the same integrated intensities for each pattern but with different unit-cell parameters [first data set; space group *R*3, unit-cell parameters $a = 82.6126\ (4)$, $c = 33.6366\ (6)$ Å]. Reflections with a reasonable signal-to-noise ratio could be observed up to a *d*-spacing resolution of approximately 3 Å [$I/\sigma(I) \simeq 2$]. This procedure allowed us to extract a set of 2140 intensities with improved effective completeness (Fig. 6), as defined elsewhere (Margiolaki, Wright, Wilmanns *et al.*, 2007). This set of intensities were employed for generating a total OMIT map based on the Bhat procedure (Bhat, 1988), as described in §6.

[1] Supplementary material has been deposited in the IUCr electronic archive (Reference: MV5084). Services for accessing this material are described at the back of the journal.

5. Rigid-body representation of amino-acid residues

An efficient way of describing the structure of a protein is implemented in *GSAS*, in which each amino acid is represented by a flexible rigid body (FRB). The origin of each FRB is the location of the C^{α} atom and the orientation is described *via* a quaternion, thus requiring six adjustable parameters. The side chain of each amino acid has adjustable torsion angles, and the orientations of the carbonyls (ψ angles) are also allowed variables for each FRB. All bond lengths and angles within each FRB are fixed at the ideal values. Restraints are then only needed for the interatomic distances and angles about the C—N coupling between amino acids along the polypeptide chain and for the torsion angles, as described previously (Von Dreele, 2007). This rigid-body model requires slightly more than a third of the number of refinable parameters in a fully free-atom refinement, thus making it better suited for Rietveld refinement of proteins. In the case of T_6 bovine insulin considered here, the number of parameters in the FRB refinement of the protein atoms only was 919, compared with the 2403 that would be needed for a free-atom refinement. Moreover, the use of idealized amino-acid bond lengths and angles in each FRB lowers the number of restraints from the 3023 required for free-atom refinement to just 1542 for FRB refinement.

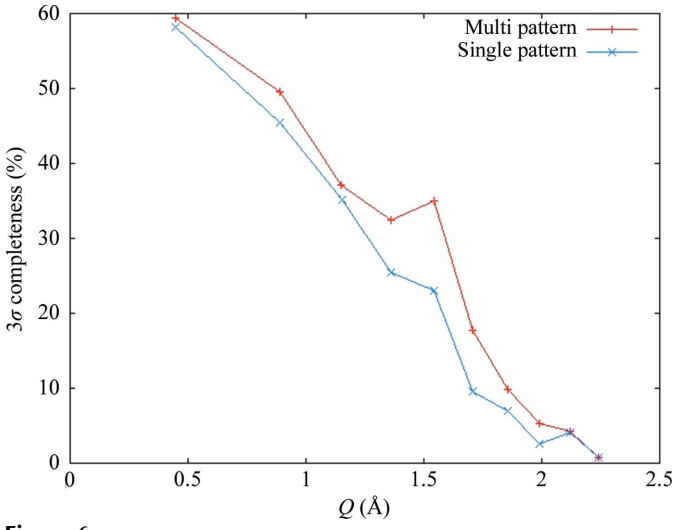

Figure 6
Effective completeness of the powder diffraction data at the 3σ level (see text) *versus* the Q range ($Q = 2\pi/d$). Blue and red colours represent single powder patterns and a combined fit to seven patterns of samples crystallized at different pH levels, respectively.

6. Detection of zinc ions and structure refinement

In the initial steps of our analysis, a total OMIT map was generated with *SFCHECK* using only the protein atoms of the model with PDB code 2a3g (Smith *et al.*, 2005) and extracted intensities from the combined Pawley fit described in §4. Inspection of the map in *Coot* immediately revealed the positions and the octahedral coordination of two zinc ions in the hexameric structure, which were added in our structural model (Fig. 7). Each zinc ion is octahedrally coordinated by three $N^{\varepsilon 2}$ atoms of three symmetry-related HisB10 residues and three symmetry-related water molecules. The detected zinc ions along with the protein atoms were then subjected to further cycles of Rietveld refinement (Rietveld, 1969). The refined $Zn-N^{\varepsilon 2}$ distances in the final stages of our analysis were 2.20 and 2.08 Å for monomers 1 and 2, respectively. These values are comparable to those reported for T_6 bovine insulin (Smith *et al.*, 2005) and T_6 porcine insulin (Baker *et al.*, 1988) of 2.06 and 2.10 Å, respectively. The Zn—OW distances are 2.41 and 2.40 Å for monomers 1 and 2, respectively (Fig. 10).

Owing to the absence of any clear indications of structural modifications *versus* pH or sample-exposure time, a 14-histogram stereochemically restrained Rietveld refinement was carried out in order to extract an average structural model for T_6 bovine insulin using the *GSAS* software. The selected profiles correspond to samples

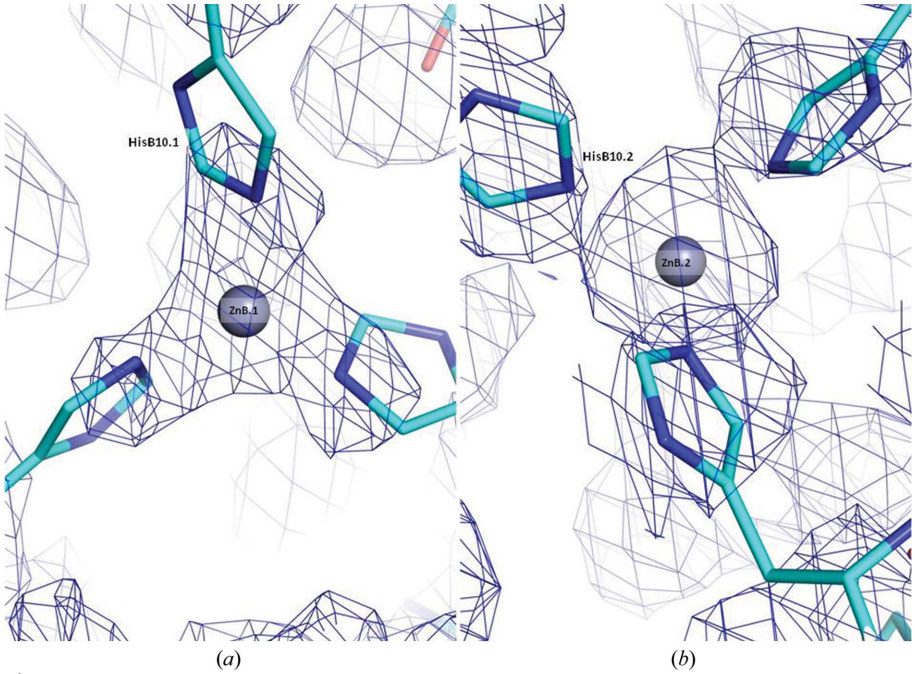

Figure 7
Selected regions of the total OMIT map at 1σ clearly indicating the positions and coordination of the two zinc ions present in T6 bovine insulin. The map was computed at the initial stages of our analysis employing only the protein atoms (excluding all ligands) from the model deposited as PDB entry 2a3g and the extracted intensities from the seven-pattern combined Pawley fit. The map was computed using *SFCHECK*. The residues represented as cyan sticks correspond to the starting model, 2a3g, and the grey spheres represent the two independent zinc ions, ZnB.1 (*a*) and ZnB.2 (*b*), which are octahedrally coordinated by three symmetry-related HisB10 side chains. This figure was generated using *PyMOL* (http://www.pymol.org/).

Table 1
Data-collection and refinement statistics using 14 high-resolution profiles of T_6 bovine insulin collected at RT (ID31, ESRF).

Details are given for three selected profiles corresponding to samples crystallized at different pH values of 5.4, 6.8 and 7.6. The profiles were collected during 60 s of sample exposure time to the synchrotron beam. In order to increase the counting statistics without compromising the data quality, identical scans collected from fresh parts of the samples were summed together as described in §2.2.

	Data set 1	Data set 2	Data set 3
Sample	pH 5.4, irradiation time 60 s	pH 6.8, irradiation time 60 s	pH 7.6, irradiation time 60 s
Data collection			
Wavelength (Å)	1.29967 (9)		
$\Delta 2\theta$ (°)	0.275 (2)		
$I/\sigma(I)$	2 at d = 3 Å		
Rietveld refinement			
Program	*GSAS*		
d-spacing range (Å)	18.2–2.7		
N_{ref}	2140	2140	2140
$N_{restraints}$	1542	1542	1542
N_{steps}	7563	5710	7587
$N_{parameters}$	1102	1102	1102
Profile scale factors	0.189 (7)	0.119 (5)	0.298 (5)
R_{wp} (%)	9.37	9.44	8.09
R_p (%)	7.06	7.50	5.99
$R(F^2)$ (%)	25.05	35.26	23.45
Total R factors for the 14 histograms	R_{wp} = 9.45%, R_p = 7.24%, $R(F^2)$ = 23.8%		
Profile parameters			
Y	8.569 (6)	8.456 (4)	11.947 (2)
Y_e	7.375 (3)	6.153 (2)	9.858 (4)
$D11$	0	−0.00445 (12)	−0.0091 (2)
$D33$	0	0.0312 (3)	0.0431 (5)
Solvent scattering coefficients via Babinet's principle model			
A_s	4.707 (11)	4.742 (12)	4.657 (11)
B_s	2.737 (8)	3.675 (9)	4.211 (7)
No. of protein atoms	800		
No. of Zn atoms	2		
No. of water molecules	44		
Model quality			
Ramachandran plot			
Most favoured (%)	95.3		
Additionally allowed (%)	4.7		
R.m.s.d., bonds (Å)	0.029		
R.m.s.d., angles (°)	1.75		

crystallized at pH 5.4, 6.0, 6.2, 6.6, 7.0 and 7.6, as well as subsequent data sets of samples crystallized at pH 5.4, 6.2 and 7.6 exhibiting radiation-induced anisotropic lattice alterations as described in §3. In this case, the diffraction profiles were included based on the observed signal-to-noise ratio, data resolution, full width at half maximum (FWHM) and relative differences in the positions of the observed reflections. The anisotropic changes in the unit cell were taken into account by using a special profile function implemented in *GSAS* (No. 5; Larson & Von Dreele, 2004). In this function only one set of lattice parameters is refined and those corresponding to the rest of the profiles are related *via* a strain ($\delta d/d$) of the reciprocal metric tensor elements. Parameters related to the strain are refined in the least-squares procedure. This type of restrained least-squares procedure has previously been successfully applied to several reference proteins (Von Dreele, 1999, 2001, 2005; Margiolaki *et al.*, 2005; Basso *et al.*, 2005; Margiolaki & Wright, 2008), a previously unknown crystalline phase of insulin (Von Dreele *et al.*, 2000) and the SH3 domain of ponsin (Margiolaki, Wright, Wilmanns *et al.*, 2007). The method is described in detail elsewhere (Von Dreele, 2007). Effectively, the use of several data sets was essential for augmenting the robustness of the structure refinement and the quality of the electron-density maps. The different data sets have slightly different lattice parameters owing to sample preparation or induced by exposure to radiation. These cause relative shifts in the positions of neighbouring peaks, thus reducing correlations between overlapping reflections, as illustrated in Figs. 3 and 5.

A total of 1542 stereochemical restraints were imposed in order to refine the positions of 800 protein atoms, two Zn atoms and 44 water molecules in the asymmetric unit using experimental data in the resolution range 18.2–2.7 Å for all profiles. A Babinet's principle modification of all the atom scattering factors according to

$$f = f_0 - A_s \exp(-8\pi^2 B_s \sin^2\theta/\lambda^2)$$

accounted for solvent scattering and facilitated fitting of the lowest angle part of the powder diffraction data. Thus, two coefficients (A_s and B_s) were refined to account for the solvent scattering. These coefficients were varied separately for each of the different patterns and they can therefore account for some of the small differences in peak intensities at low angles between the different profiles. The initial model, including the protein atoms of the model with PDB code 2a3g and the detected zinc ions from total OMIT maps, provided a moderate fit to the powder data [total agreement factors: R_{wp} = 17.6% and $R(F^2)$ = 34%].

Periodical evaluations of the protein stereochemistry were crucial for monitoring the progress of the refinement, and various validation programs, including *PROCHECK* (Laskowski *et al.*, 1993), *SFCHECK* (Vaguine *et al.*, 1999), *ERRAT* (Colovos & Yeates, 1993) and *WHAT_CHECK* (Hooft *et al.*, 1996), were used. In summary, after merging all 14 data sets and extracting the calculated structure factors during the Rietveld refinement, the program *SFCHECK* was employed to evaluate them against the observed structure factors. In the same procedure in *SFCHECK*, a total OMIT map was generated. Visual inspection of the refined model against the OMIT map was performed in *Coot* v.0.7 (Emsley & Cowtan, 2004; Emsley *et al.*, 2010). Periodically, side-chain rotamers and displacement of small groups of main-chain atoms were adjusted in order to fit the total OMIT maps and preserve good stereochemistry and the refinement was repeated. Graphical examination, energy minimization and manual rebuilding of the protein molecule were performed using

Swiss-PdbViewer (Guex & Peitsch, 1997) and *Coot*. The refinement proceeded smoothly for the 14 profiles, leading to a good quality of the final fit [total agreement factors: R_{wp} = 9.45%, R_p = 7.24%, $R(F^2)$ = 23.8%]. Details of the refinement statistics are listed in Table 1 and the final fits to three of the 14 profiles are shown in Fig. 8. Fig. 9 shows a ribbon diagram depicting the backbone arrangement of the refined structure generated in *PyMOL* (v.1.2r3pre; Schrödinger). The gradual modification of the orientation and position of individual amino acids during the refinement procedure is shown in Supplementary Fig. S1.

Selected regions of the refined coordinates and total OMIT map computed at the final steps of analysis are presented in Fig. 10. The powder diffraction model is virtually identical to that obtained from single-crystal measurements (PDB entry 2a3g), with a mean main-chain root-mean-square displacement (r.m.s.d.) for the four protein chains in the asymmetric unit of 0.34 Å and a mean side-chain r.m.s.d. of 0.77 Å. The distribution of the r.m.s.d. values *versus* residue number for chains A and B of the two protein monomers existing in the asymmetric unit, as derived using *LSQKAB* (Winn *et al.*, 2011), is illustrated in Supplementary Fig. S2. The mean r.m.s.d. values are 0.32 and 0.56 Å for the main-chain and side-chain atoms of chain A.1; 0.37 and 0.90 Å for the main-chain and side-chain atoms of chain B.1; 0.32 and 0.68 Å for the main-chain and side-chain atoms of chain A.2; and 0.36 and 0.93 Å for the main-chain and side-chain atoms of chain B.2, respectively. The complete list of values indicates that the largest deviations are observed in certain side-chain atoms of chains B.1 and B.2 which include the two zinc ions in the asymmetric unit. This could be interpreted in terms of slightly different Zn sites between the single-crystal and powder models, resulting in displacement of the neighbouring protein residues. The water molecules were compared using *Coot*. Despite the different resolution limits for the powder and single-crystal data, 44 out of 56 water molecules are in good agreement.

7. Discussion

In the present study, we exploit the effects of pH and sample-irradiation time on the T_6 hexameric crystal form of bovine insulin in order to resolve overlapping reflections present in the collected profiles. We have made accurate measurements of the evolution of the lattice parameters with pH and irradiation time (Fig. 4), which are illustrated by smooth anisotropic shifts in the peak positions (Figs. 3 and 5). The reproducibility of these results and the precision of the powder diffraction data have been verified by repeating measurements on the ID31 and ID11 beamlines of the ESRF. As a result of the systematic changes in the unit-cell parameters, we believe that the observed variation is an intrinsic property of bovine insulin. Analogous behaviour has been

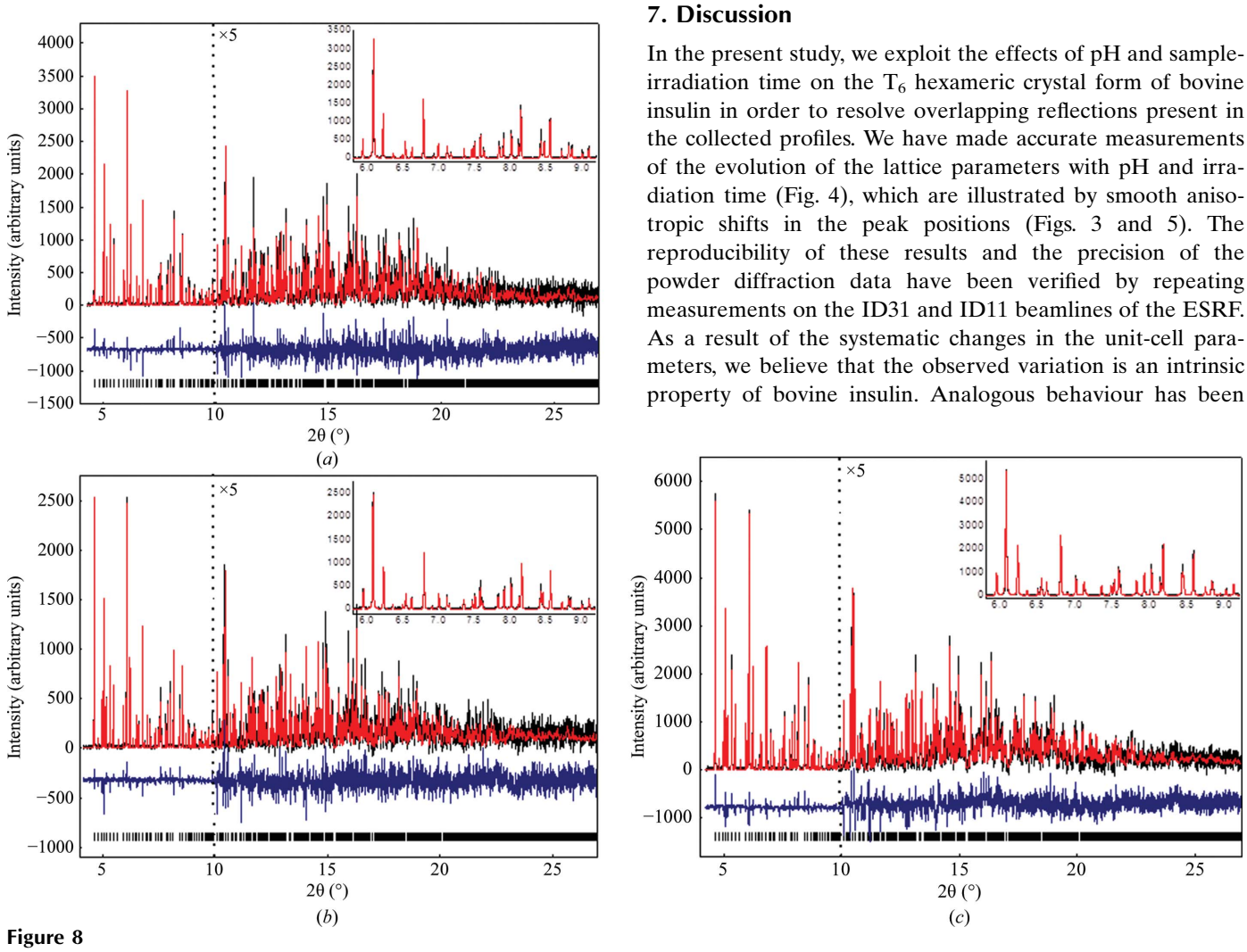

Figure 8
Final fits of three of the 14 data sets employed in a combined stereochemically restrained Rietveld analysis. The data for samples crystallized at pH 5.4 (*a*), pH 6.8 (*b*) and pH 7.6 (*c*) were collected at 295 K [ID31, λ = 1.29967 (9) Å]. The black, red and lower black lines represent the experimental data, the calculated pattern and the difference between the experimental and calculated profiles, respectively. The vertical bars correspond to Bragg reflections compatible with the refined hexagonal structural model. The profiles have been expanded by a factor of five at Bragg angles larger than 10°. Insets, magnification of the 5.8–9.2° 2θ regime. The background intensity has been subtracted for clarity. Details of the Rietveld analysis are listed in Table 1.

observed for tetragonal hen egg-white lysozyme (HEWL; Basso *et al.*, 2005; Von Dreele, 2007) and human insulin (Karavassili *et al.*, 2012). The changes in unit-cell parameters observed in tetragonal HEWL on varying the temperature of data collection during single-crystal diffraction experiments have been attributed to both slight conformational changes and solvent rearrangements (Kurinov & Harrison, 1995). Similar volume modifications to those reported here have been observed for orthorhombic HEWL on varying the humidity and as a consequence the solvent content in the unit cell (Sukumar *et al.*, 1999), and in different enzymes such as *Rhizopus* pepsin, in which both conformational and water-structure changes were observed with varying pH (Prasad & Suguna, 2003). Moreover, we recently reported analogous anisotropic lattice alterations with increasing pH and irradiation time for distinct crystalline polymorphs of rasburicase, a recombinant urate oxidase enzyme (Uox) from *Aspergillus flavus* (Collings *et al.*, 2010).

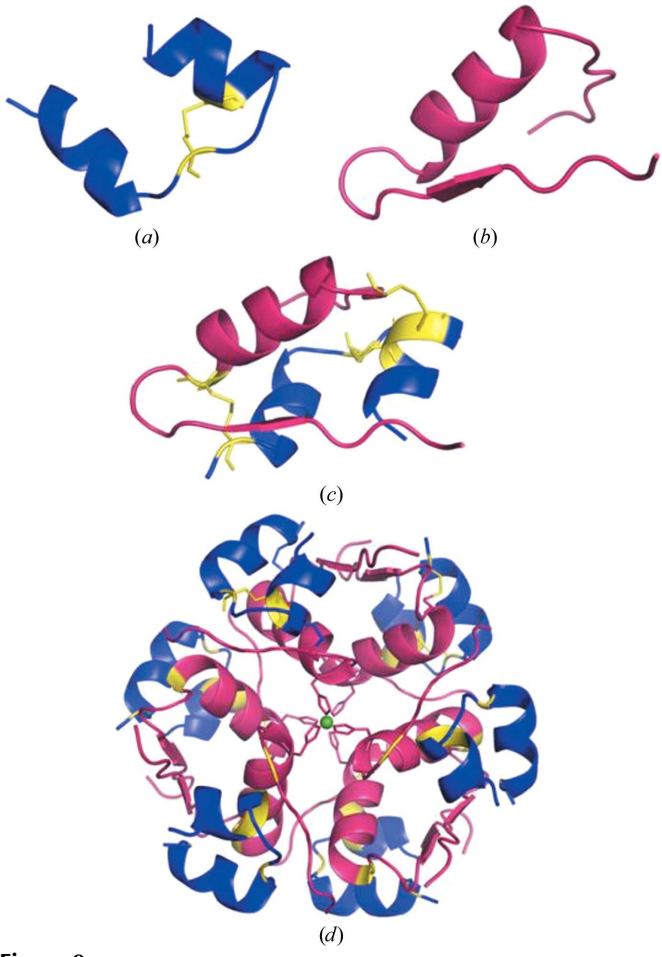

Figure 9
Powder-diffraction structure of the T_6 bovine insulin hexamer. Bovine insulin consists of two chains: A (21 amino acids) shown in blue (*a*) and B (30 amino acids) shown in purple (*b*). Chain A contains a disulfide between CysA6 and CysA11 (shown in yellow). The chains are held together by two disulfide bonds (shown in yellow) in order to form a monomer (*c*). Finally, the T6 hexamer is shown in (*d*). The C^{α} trace is viewed down the crystallographic threefold axis. The zinc ions are shown as green spheres. Each of the two independent zinc ions is octahedrally coordinated by three HisB10 side chains (shown in purple). Because both Zn atoms lie on the threefold axis, only one is visible in the figure. This figure was generated using *PyMOL* (http://www.pymol.org/).

The molecular structure is obtained *via* a 14-pattern stereochemically restrained Rietveld refinement which exploits the anisotropic variations in unit-cell parameters to reduce the effects of the peak-overlap problem. An efficient way of describing the structure of a protein is presented, in which each amino acid is represented by a flexible rigid body (FRB). The FRB approach requires a significantly smaller number of refinable parameters and restraints than a fully free-atom refinement. This method definitely increases the robustness of the refinement in comparison to the free-atom refinements reported to date, and this will be discussed in a subsequent article.

Our estimates of the data quality and completeness indicate that this methodology provides considerable improvements compared with the use of a single diffraction pattern. In addition, we have observed that the combination of multiple profiles in the same Rietveld analysis leads to higher robustness of the least-squares procedure. Analysis of the intensity residuals after refinement showed that the differences between the 14 patterns (corresponding to different samples and/or sample-irradiation times) are smaller than the difference between the model and any of the profiles, which validates the use of the combined refinement. Variations of the peak intensities as a function of pH were accounted for by variations in the bulk-solvent parameters, which are difficult to interpret at an atomic level. Our refined structure is similar in topology and stereochemistry to the previously determined structure obtained from single-crystal data (Smith *et al.*, 2005). The largest deviations from the previous structure occur in the flexible side chains of certain residues in chains B.1 and B.2 associated with the Zn atoms present in the structure. Additional slight differences between the present structure and other conformations can be attributed to the fact that in this case an average model has been derived for the description of T_6 bovine insulin throughout the pH region under study. With the limited resolution of the data, the maps obtained using structure factors extracted from the individual powder datasets did not reveal any structural modifications with increasing pH from 5.0 to 7.6.

The variation of the unit-cell volume with pH is smaller than the anisotropic distortion, indicating that the changes are more likely to be the consequence of a rearrangement of the unit-cell contents rather than the introduction of another chemical species. In the crystal structure the molecules are held together by intermolecular contacts, with solvent channels filling the spaces between them. The largest solvent channels in T_6 bovine insulin are oriented parallel to the crystallographic *c* axis. Each of the two independent zinc ions is octahedrally coordinated by three symmetry-related HisB10 side chains and three symmetry-related water molecules (Figs. 7 and 10). As has been observed in human, porcine and bovine insulin, the GluB13 side chains are directed towards the centre of the hexamer, where a short contact of 2.65 Å occurs between two independent carboxyl O atoms, again suggesting the presence of a centred hydrogen bond. The side

chains of the three A10 residues in one trimer make van der Waals contacts with the A10 side chains in a translationally related hexamer (Smith *et al.*, 2005). It seems plausible that the localized changes in molecular charge distribution caused by the titration of charged groups on these side chains may modify the strength of the intermolecular interactions and could be manifested in the change in unit-cell parameters that we observe with increasing pH. It is beyond the scope of the present study to refine the structures resulting from the different pH conditions individually; however, minor localized changes in the lattice contacts involving these residues may arise in structures at pH 5.0 and 7.6. Several previous reports have suggested that net changes in surface-charge distribution induced by fine increments in pH influence nucleation rates (McPherson, 1982) as well as crystal size and axial ratios (Judge *et al.*, 1999).

We believe that this kind of systematic approach further extends the viability of powder diffraction methods for research on macromolecular systems. In the present study 14 samples were measured *via* an automated procedure in less than 7 h, providing extremely high-quality powder data. The low instrumental contribution to the diffraction lines and the high precision of the determination of the lattice parameters has allowed small variations in the unit-cell dimensions with varying pH to be quantified precisely. The use of a systematic variation of sample-preparation conditions has been particularly useful for the detection of protein–ligand complex formation by variations of ligand concentration (Von Dreele, 2001, 2005), the identification of subsequent phase transitions with increasing pH in the case of human insulin (Karavassili *et al.*, 2012) and the structure solution of the previously unknown SH3 domain of ponsin (Margiolaki, Wright, Wilmanns *et al.*, 2007). The optimization of cryoprotection conditions and the preparation of heavy-atom derivatives could also exploit systematic powder experiments, as demonstrated in previous studies on hen egg-white lysozyme and porcine pancreatic elastase (Besnard *et al.*, 2007; Wright *et al.*, 2008; Basso *et al.*, 2010).

In conclusion, we have observed systematic variations in the hexagonal unit cell of bovine insulin as a function of the pH

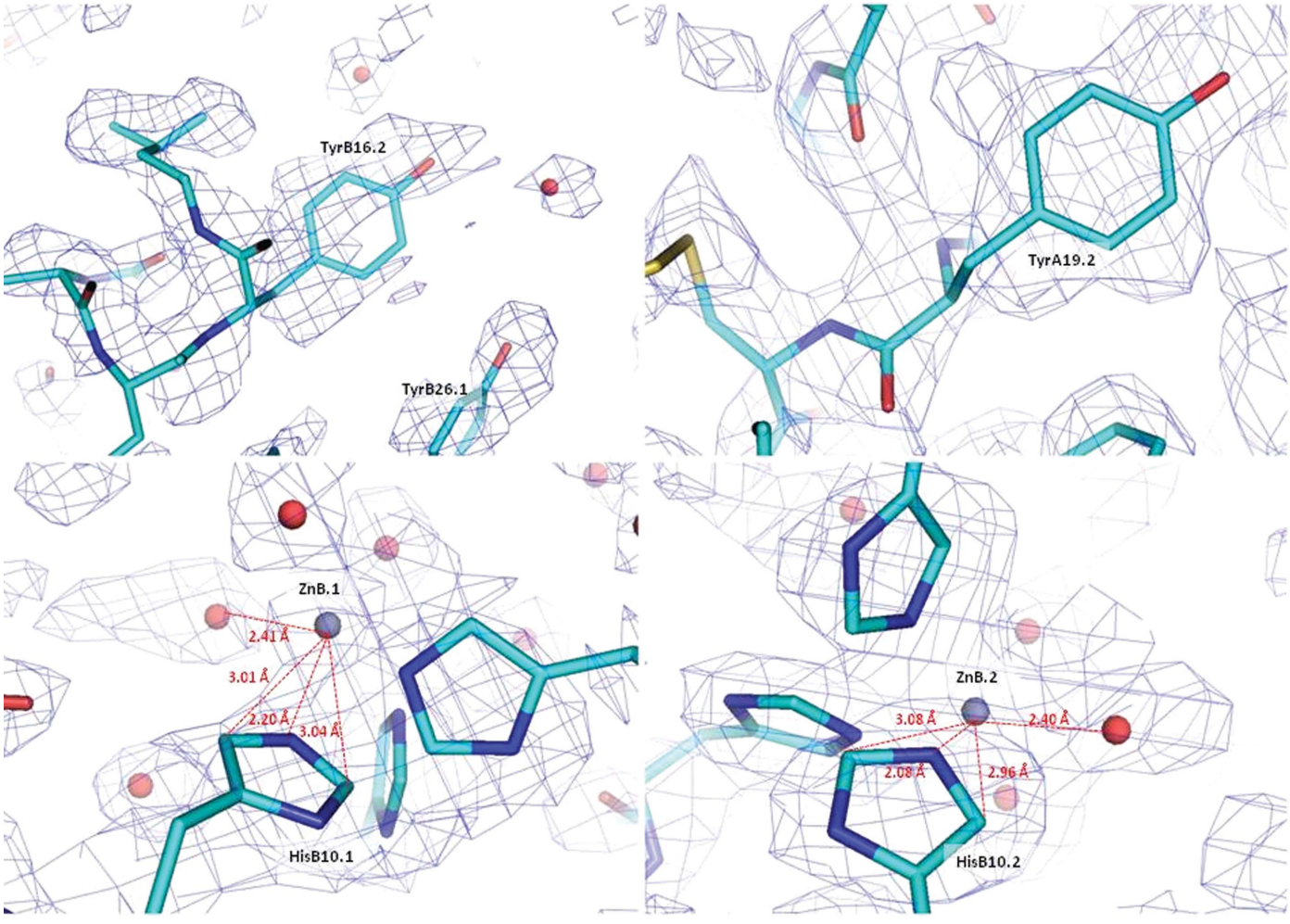

Figure 10
Selected regions of the final refined structural model in stick representation and the corresponding OMIT map contoured at 1σ. The cyan, blue and red colours in the stick representation illustrate C, N and O atoms of individual amino acids. The grey spheres represent the two independent Zn atoms and the red spheres denote water molecules identified during analysis. The closest distances between the two Zn ions and the neighbouring His atoms and water molecules are indicated in red. This figure was generated using *PyMOL* (http://www.pymol.org/).

used for crystallization at RT as well as increasing irradiation time. This result might be indicative of solvent rearrangements, slight changes in the protein conformation or changes in packing contacts. While the powder data give clear results pertaining to the unit-cell parameters, the electron density is not of sufficiently high quality to distinguish between these possibilities. We were able to account for the data at all pH values without any conformational rearrangements, although this possibility cannot be ruled out. At the current level of analysis our observations are consistent with the changes in unit-cell dimensions being the result of a reorganization of the water structure, which is anticipated to have an effect on the unit-cell dimensions of the same order of magnitude and would be consistent with the observed changes in the bulk-solvent parameter; however, minor modifications in specific packing contacts may also be a contributing factor and may well be linked to reorganization of the water structure by changing the dimensions of specific solvent channels.

We would like to thank the ESRF for the provision of beam time at the ID31 and ID11 beamlines. We thank Gavin C. Fox for his valuable suggestions related to the crystallization experiments presented here and Spyros Chatziefthimiou for useful advice. We thank both reviewers for their constructive suggestions. IM is grateful to the UNESCO–L'Oreal foundations for the award of the International Fellowship for Women in Life Sciences (2010–2012). This research has been co-financed by the European Union (European Regional Development Fund – ERDF) and Greek national funds through the Operational Program 'Regional Operational Programme' of the National Strategic Reference Framework (NSRF) – Research Funding Program: Support for Research, Technology and Innovation Actions in Region of Western Greece. Work at the Advanced Photon Source was supported by the US Department of Energy, Office of Science, Office of Basic Energy Sciences under Contract No. DE-AC02-06CH11357. Finally, the EU FP7 REGPOT CT-2011-285950 'SEEDRUG' project and the NanoMEGAS company supported this work.

References

Baker, E. N., Blundell, T. L., Cutfield, J. F., Cutfield, S. M., Dodson, E. J., Dodson, G. G., Hodgkin, D. M., Hubbard, R. E., Isaaccs, N. W. & Reynolds, C. D. (1988). *Philos. Trans. R. Soc. London Ser. B*, **319**, 369–456.

Basso, S., Besnard, C., Wright, J. P., Margiolaki, I., Fitch, A., Pattison, P. & Schiltz, M. (2010). *Acta Cryst.* D**66**, 756–761.

Basso, S., Fitch, A. N., Fox, G. C., Margiolaki, I. & Wright, J. P. (2005). *Acta Cryst.* D**61**, 1612–1625.

Besnard, C., Camus, F., Fleurant, M., Dahlstrom, A., Wright, J. P., Margiolaki, I., Pattison, P. & Schiltz, M. (2007). *Z. Kristallogr. Suppl.* **26**, 39–44.

Bhat, T. N. (1988). *J. Appl. Cryst.* **21**, 279–281.

Boultif, A. & Louër, D. (1991). *J. Appl. Cryst.* **24**, 987–993.

Ciszak, E. & Smith, G. D. (1994). *Biochemistry*, **33**, 1512–1517.

Collings, I., Watier, Y., Giffard, M., Dagogo, S., Kahn, R., Bonneté, F., Wright, J. P., Fitch, A. N. & Margiolaki, I. (2010). *Acta Cryst.* D**66**, 539–548.

Colovos, C. & Yeates, T. O. (1993). *Protein Sci.* **2**, 1511–1519.

David, W. I. F., Shankland, K. & Shankland, N. (1998). *Chem. Commun.* **8**, 931–932.

Derewenda, U., Derewenda, Z., Dodson, E. J., Dodson, G. G., Reynolds, C. D., Smith, G. D., Sparks, C. & Swenson, D. (1989). *Nature (London)*, **338**, 594–596.

Emsley, P. & Cowtan, K. (2004). *Acta Cryst.* D**60**, 2126–2132.

Emsley, P., Lohkamp, B., Scott, W. G. & Cowtan, K. (2010). *Acta Cryst.* D**66**, 486–501.

Fitch, A. (2004). *J. Res. Natl Inst. Stand. Technol.* **109**, 133.

Garman, E. (1999). *Acta Cryst.* D**55**, 1641–1653.

Garman, E. & Nave, C. (2002). *J. Synchrotron Rad.* **9**, 327–328.

Guex, N. & Peitsch, M. C. (1997). *Electrophoresis*, **18**, 2714–2723.

Hammersley, A. P. (1997). ESRF Internal Report ESRF 97HA02T.

Helliwell, J. R., Bell, A. M. T., Bryant, P., Fisher, S., Habash, J., Helliwell, M., Margiolaki, I., Kaenket, S., Watier, Y., Wright, J. P. & Yalamanchilli, S. (2010). *Z. Kristallogr.* **225**, 570–575.

Hooft, R. W., Vriend, G., Sander, C. & Abola, E. E. (1996). *Nature (London)*, **381**, 272.

Huang, T. C., Toraya, H., Blanton, T. N. & Wu, Y. (1993). *J. Appl. Cryst.* **26**, 180–184.

Jenner, M. J., Wright, J. P., Margiolaki, I. & Fitch, A. N. (2007). *J. Appl. Cryst.* **40**, 121–124.

Judge, R. A., Jacobs, R. S., Frazier, T., Snell, E. H. & Pusey, M. L. (1999). *Biophys. J.* **77**, 1585–1593.

Kaarsholm, N. C., Ko, H. C. & Dunn, M. F. (1989). *Biochemistry*, **28**, 4427–4435.

Karavassili, F., Giannopoulou, A. E., Kotsiliti, E., Knight, L., Norrman, M., Schluckebier, G., Drube, L., Fitch, A. N., Wright, J. P. & Margiolaki, I. (2012). *Acta Cryst.* D**68**, 1632–1641.

Kurinov, I. V. & Harrison, R. W. (1995). *Acta Cryst.* D**51**, 98–109.

Labiche, J. C., Mathon, O., Pascarelli, S., Newton, M. A., Ferre, G. G., Curfs, C., Vaughan, G., Homs, A. & Carreiras, D. F. (2007). *Rev. Sci. Instrum.* **78**, 091301.

Larson, A. C. & Von Dreele, R. B. (2004). Los Alamos National Laboratory Report LAUR 86-748.

Laskowski, R. A., MacArthur, M. W., Moss, D. S. & Thornton, J. M. (1993). *J. Appl. Cryst.* **26**, 283–291.

Margiolaki, I. & Wright, J. P. (2008). *Acta Cryst.* A**64**, 169–180.

Margiolaki, I., Wright, J. P., Fitch, A. N., Fox, G. C., Labrador, A., Von Dreele, R. B., Miura, K., Gozzo, F., Schiltz, M., Besnard, C., Camus, F., Pattison, P., Beckers, D. & Degen, T. (2007). *Z. Kristallogr. Suppl.* **26**, 1–13.

Margiolaki, I., Wright, J. P., Fitch, A. N., Fox, G. C. & Von Dreele, R. B. (2005). *Acta Cryst.* D**61**, 423–432.

Margiolaki, I., Wright, J. P., Wilmanns, M., Fitch, A. N. & Pinotsis, N. (2007). *J. Am. Chem. Soc.* **129**, 11865–11871.

McPherson, A. (1982). *Preparation and Analysis of Protein Crystals*, pp. 98–99. New York: John Wiley.

Norrman, M. (2007). PhD thesis. Lund University, Sweden.

Norrman, M., Ståhl, K., Schluckebier, G. & Al-Karadaghi, S. (2006). *J. Appl. Cryst.* **39**, 391–400.

Pawley, G. S. (1981). *J. Appl. Cryst.* **14**, 357–361.

Prasad, B. V. L. S. & Suguna, K. (2003). *Acta Cryst.* D**59**, 1755–1761.

Ravelli, R. B. G., Theveneau, P., McSweeney, S. & Caffrey, M. (2002). *J. Synchrotron Rad.* **9**, 355–360.

Richards, J. P., Stickelmeyer, M. P., Frank, B. H., Pyle, S., Barbeau, M., Radziuk, J., Smith, G. D. & DeFelippis, M. R. (1999). *J. Pharm. Sci.* **88**, 861–867.

Rietveld, H. M. (1969). *J. Appl. Cryst.* **2**, 65–71.

Seigler, D. E., Olsson, G. M., Agramonte, R. F., Lohman, V. L., Ashby, M. H., Reeves, M. L. & Skyler, J. S. (1991). *Diabetes Nutr. Metab.* **4**, 267–273.

Smith, G. D. & Dodson, G. G. (1992). *Proteins*, **14**, 401–408.

Smith, G. D., Pangborn, W. A. & Blessing, R. H. (2003). *Acta Cryst.* D**59**, 474–482.

Smith, G. D., Pangborn, W. A. & Blessing, R. H. (2005). *Acta Cryst.* D**61**, 1476–1482.

Sukumar, N., Biswal, B. K. & Vijayan, M. (1999). *Acta Cryst.* D**55**, 934–937.
Toby, B. H. (2001). *J. Appl. Cryst.* **34**, 210–213.
Vaguine, A. A., Richelle, J. & Wodak, S. J. (1999). *Acta Cryst.* D**55**, 191–205.
Vaughan, G. B. M., Wright, J. P., Bytchkov, A., Rossat, M., Gleyzolle, H., Snigireva, I. & Snigirev, A. (2011). *J. Synchrotron Rad.* **18**, 125–133.
Von Dreele, R. B. (1999). *J. Appl. Cryst.* **32**, 1084–1089.
Von Dreele, R. B. (2001). *Acta Cryst.* D**57**, 1836–1842.
Von Dreele, R. B. (2003). *Methods Enzymol.* **368**, 254–267.
Von Dreele, R. B. (2005). *Acta Cryst.* D**61**, 22–32.
Von Dreele, R. B. (2006). *J. Appl. Cryst.* **39**, 124–126.
Von Dreele, R. B. (2007). *J. Appl. Cryst.* **40**, 133–143.
Von Dreele, R. B., Stephens, P. W., Smith, G. D. & Blessing, R. H. (2000). *Acta Cryst.* D**56**, 1549–1553.
Watier, Y. (2011). PhD thesis. ESRF and Université de Grenoble, France.
Watier, Y., Margiolaki, I., Wright, J., Fitch, A., Norrman, M. & Schluckebier, G. (2009). *Acta Cryst.* A**65**, s320–s321.
Whittingham, J. L., Chaudhuri, S., Dodson, E. J., Moody, P. C. & Dodson, G. G. (1995). *Biochemistry*, **34**, 15553–15563.
Winn, M. D. *et al.* (2011). *Acta Cryst.* D**67**, 235–242.
Wright, J. P., Besnard, C., Margiolaki, I., Basso, S., Camus, F., Fitch, A. N., Fox, G. C., Pattison, P. & Schiltz, M. (2008). *J. Appl. Cryst.* **41**, 329–339.
Wright, J. P. & Forsyth, J. B. F. (2000). Rutherford Appleton Laboratories Report RAL-TR-2000-012.